POLYMER ENGINEERING

High thermal conductivity in electrostatically engineered amorphous polymers

Apoorv Shanker,[1]* Chen Li,[2]* Gun-Ho Kim,[2,3,4] David Gidley,[5] Kevin P. Pipe,[2,6]† Jinsang Kim[1,4,7,8]†

High thermal conductivity is critical for many applications of polymers (for example, packaging of light-emitting diodes), in which heat must be dissipated efficiently to maintain the functionality and reliability of a system. Whereas uniaxially extended chain morphology has been shown to significantly enhance thermal conductivity in individual polymer chains and fibers, bulk polymers with coiled and entangled chains have low thermal conductivities (0.1 to 0.4 W m^{-1} K^{-1}). We demonstrate that systematic ionization of a weak anionic polyelectrolyte, polyacrylic acid (PAA), resulting in extended and stiffened polymer chains with superior packing, can significantly enhance its thermal conductivity. Cross-plane thermal conductivity in spin-cast amorphous films steadily grows with PAA degree of ionization, reaching up to ~1.2 W m^{-1} K^{-1}, which is on par with that of glass and about six times higher than that of most amorphous polymers, suggesting a new unexplored molecular engineering strategy to achieve high thermal conductivities in amorphous bulk polymers.

INTRODUCTION

Effective thermal management in applications such as batteries, automobile cooling systems, and high–power density electronic devices, where heat accumulation can have deleterious effects, is critically important to ensure system performance and reliability and to enhance lifetime. Despite their poor thermal conductivity (κ), various advantages, including light weight, low cost, and easy processability, make polymers the material of choice for several heat-intensive applications such as electronic chip encapsulation, cell phone casing, and LED (light-emitting diode) housing. These existing applications, along with emerging technologies such as flexible electronics, for which the requirements on flexibility and light weight cannot be met by most conventional thermal management materials (metals and ceramics), put greater technological incentives on developing thermally conductive polymers.

Blending with high-κ fillers such as metal or ceramic particles, carbon nanotubes (CNTs), or graphene flakes is the most commonly used method to enhance polymers' thermal conductivity (*1*). However, the large volume fraction of fillers required to achieve appreciable enhancement in κ often leads to undesired optical or electrical properties, increased weight, high cost [for example, ~$1000/kg for CNT versus ~$2/kg for poly(methyl methacrylate)], or loss of the easy processability generally associated with polymers.

In contrast to low κ in bulk samples, constituent individual polymer chains are believed to have large κ. The thermal conductivity of a single polymer chain, in which the elastic disorder (*2*) between intrachain covalent and interchain van der Waals bonds is absent, was calculated to be as large as few hundreds of watts per meter per kelvin (*3*). Ultradrawn crystalline nanofibers with aligned polymer chains were measured to have κ of more than 100 W m^{-1} K^{-1} in the alignment direction (*4*). The large thermal conductivities of single- or few-chain fibers can be retained in amorphous polymers in the direction of chain orientation (*5*, *6*), along which heat propagation occurs predominantly through intrachain transport. Singh *et al.* (*7*) reported a significant increase in κ in amorphous polythiophene fabricated via a nanotemplate-assisted electrochemical method that allows polythiophene chains to be oriented in the vertical direction. Thermal conductivity greater than 2 W m^{-1} K^{-1} has been similarly reported for covalently grafted poly(3-methyl thiophene) brushes. Covalent grafting led to enhanced chain alignment as well as reduced energetic and positional disorder in these surface-grafted films (*8*). These high thermal conductivities reported in polymers with extended chain conformation stand in contrast to surface-grown polymer brushes (*9*) and polymer films under high pressure (*10*), in which the coiled conformation of polymer chains likely remained and enhancement in κ was found to be relatively moderate. However, these approaches either limit the orientation of chain extension to a certain direction or pose challenges in terms of scaling up the nanoscale films for practical applications. Therefore, it is desirable to achieve high κ in both in- and out-of-plane directions in bulk amorphous polymers using common fabrication processes.

Although the mechanisms of thermal transport in amorphous materials continue to be studied (*10*–*13*), it is generally believed that the thermal conductivity in bulk amorphous polymers (a class of disordered solids) is inhibited by the following: (i) highly coiled and entangled intrachain structure, (ii) loose chain packing with voids that dampen the speed at which vibrations propagate, and (iii) weak nonbonding interchain interactions (for example, van der Waals and dipole-dipole) (*14*). Here, we demonstrate an unexplored molecular engineering route that simultaneously attacks these three bottlenecks. By using the coulombic repulsive forces between ionized pendant groups on the backbone of polyelectrolytes to "stretch" the main chain at the molecular level, we achieve significant enhancements of thermal conductivity in amorphous polymer with randomly oriented yet superiorly packed extended polymer chains and strong ionic interchain interactions (Fig. 1A).

RESULTS

Thermal conductivity measurement

To test our idea, we used a weak polyelectrolyte, polyacrylic acid (PAA; atactic), made up of a C–C backbone with a carboxylic acid

[1]Department of Macromolecular Science and Engineering, University of Michigan, Ann Arbor, MI 48109–2800, USA. [2]Department of Mechanical Engineering, University of Michigan, Ann Arbor, MI 48109–2125, USA. [3]Department of Mechanical and Nuclear Engineering, Ulsan National Institute of Science and Technology, Ulsan 44919, Republic of Korea. [4]Department of Materials Science and Engineering, University of Michigan, Ann Arbor, MI 48109–2117, USA. [5]Department of Physics, University of Michigan, Ann Arbor, MI 48109–1040, USA. [6]Department of Electrical Engineering and Computer Science, University of Michigan, Ann Arbor, MI 48109–2122, USA. [7]Department of Chemistry, University of Michigan, Ann Arbor, MI 48109–1055, USA. [8]Department of Chemical Engineering, University of Michigan, Ann Arbor, MI 48109–2136, USA.
*These authors contributed equally to this work.
†Corresponding author. Email: pipe@umich.edu (K.P.P.); jinsang@umich.edu (J.K.)

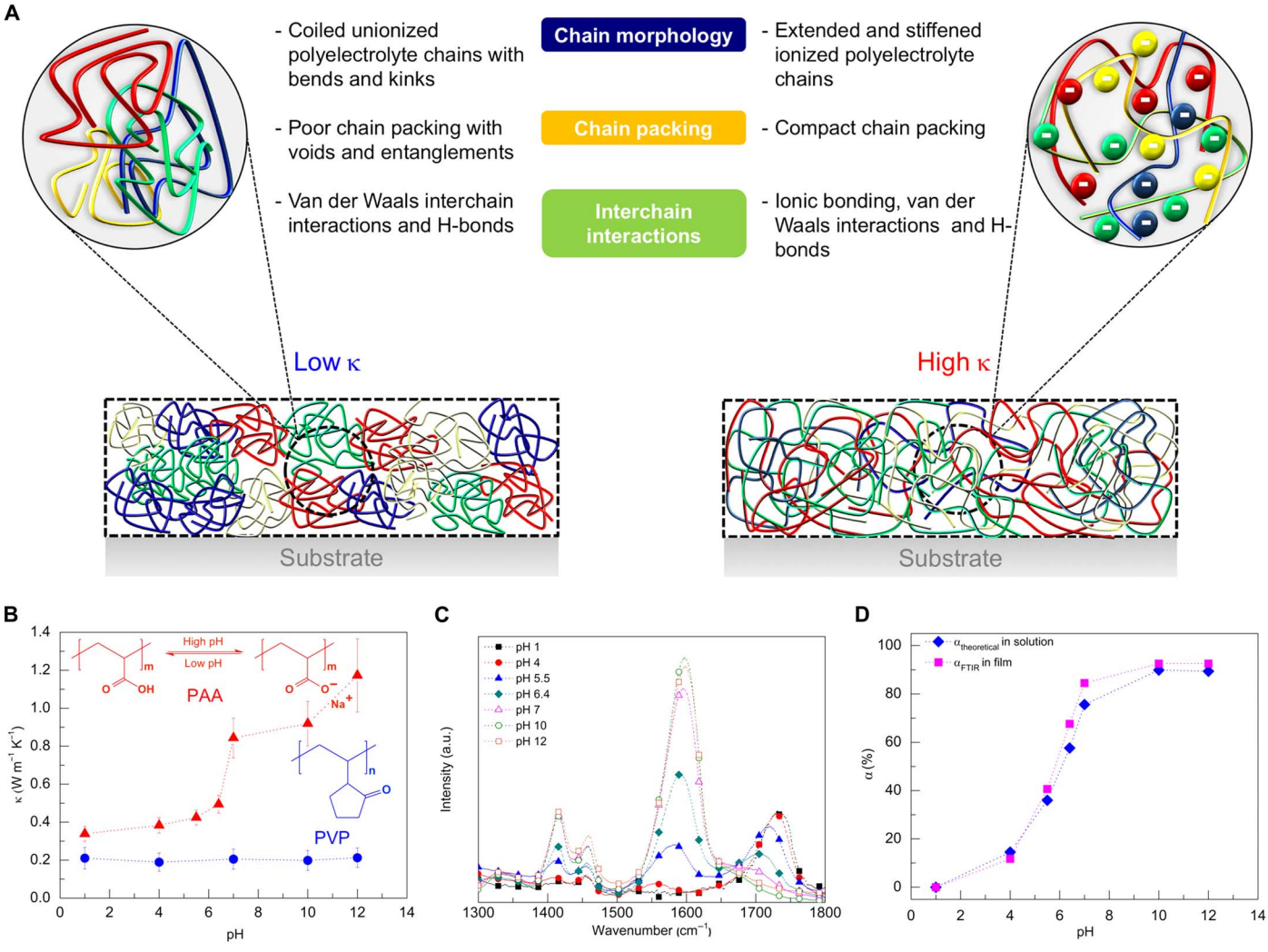

Fig. 1. High thermal conductivity in polyelectrolyte thin films via controlled ionization. (**A**) Illustrations of chain conformation and packing in spin-cast polymer films: coiled unionized polyelectrolyte (left) and extended ionized polyelectrolyte (right). The zoomed-in images show chain conformation at the molecular level. (**B**) Cross-plane thermal conductivity of a weak polyelectrolyte, PAA [molecular weight (MW), 100,000], and a nonionizable water-soluble polymer, PVP (MW, 40,000), thin films spin-cast from polymer solutions of different pH. Error bars were calculated on the basis of uncertainties in film thickness, temperature coefficient of electrical resistance for the heater, and heater width. Chemical structures of the polymers and ionization reaction for PAA are also shown. (**C**) Fourier transform infrared (FTIR) spectra of PAA films spin-cast from solutions of different pH. (**D**) Fraction of ionized carboxylic acid groups (α) as a function of solution pH: calculated from the FTIR spectra and by applying charge balance on PAA solutions.

(–COOH) group at alternate carbon atoms that can be ionized to a carboxylate ($–COO^-$) by the addition of a base, that is, with increase of the polymer solution pH. The close proximity of the densely packed ionizable groups to the polymer main chain allows the effect of electrostatic repulsion between them to easily translate to the backbone, resulting in chain extension with increasing ionization. As a negative control, a water-soluble polymer, poly(*N*-vinyl pyrrolidone) (PVP; atactic), without an ionizable pendant group, was used. To fabricate thin films for thermal conductivity measurement, we dissolved the polymer in deionized (DI) water, and the pH of the solution was adjusted to the desired value by the addition of 1 M hydrochloric acid (HCl) or 1 M sodium hydroxide (NaOH) solution. The final polymer concentrations were 0.5 and 1 weight % (wt %) for PAA and PVP, respectively. Polymer solutions were then spin-cast on a Si wafer with a ~100 nm oxide layer and were annealed to obtain smooth films with thickness ranging from 10 to 35 nm. Cross-plane thermal conductivities of the polymer films were measured by a differential 3ω method, which is a standard technique for these measurements in films with thicknesses as small as few nanometers (figs. S1 to S3) (*15*, *16*). As shown in Fig. 1B, the thermal conductivity of PAA increased from 0.34 ± 0.04 W m^{-1} K^{-1} at pH 1, when the PAA chains are completely unionized, to 1.17 ± 0.19 W m^{-1} K^{-1} at pH 12, when the PAA chains are predominantly ionized (>90%, vide infra). However, the thermal conductivity of PVP measured ~0.2 W m^{-1} K^{-1} across the entire pH range, consistent with its nonelectrolyte nature.

Polymer characterization

FTIR spectroscopy was used to confirm and quantify the extent of ionization of PAA. Figure 1C shows the FTIR spectra of PAA films spin-cast from solutions of different pH. The decrease in intensity of the carbonyl (–C=O) stretching band (1680 to 1730 cm^{-1}) of the carboxylic acid (–COOH) group with pH and the concomitant increase

in the intensity of the asymmetric carboxylate ($-COO^-$) stretching band (1556 to 1594 cm^{-1}) indicate ionization of the PAA chains (*17*). The degree of ionization (α) of PAA as a function of solution pH (Fig. 1D), calculated from the areal ratio of peaks corresponding to ionized and unionized acidic groups fitted assuming Gaussian distributions and the same extinction coefficient for the two bands (fig. S4) (*18*), matches with previously reported trends (*17*). A theoretical charge balance calculation for the PAA solution yielded similar values for α, confirming that PAA retains its ionization in the thin-film state (see the Supplementary Materials). The FTIR spectra of PVP at different values of pH are nearly identical, consistent with its nonelectrolyte nature (fig. S5A).

We further measured viscosities of PAA solutions at different pH and elastic moduli and porosities of PAA thin films fabricated from solutions at different pH to quantify the three ionization-induced effects, namely, polymer chain extension (*19*), chain stiffening (*20*), and chain packing (*19*), respectively. As shown in Fig. 2A, the relative viscosity, η_r ($=\eta_{polymer}/\eta_{water}$; $\eta_{water} = 10^{-3}$ Pa·s), increases with solution pH, indicating that coulombic repulsion between ionized carboxylic acid groups stretches out the PAA chains, resulting in an extended morphology and, hence, increased solution viscosity (*21*). Under the same spin-casting conditions, the trend in film thickness (d_f) matches well with that of solution viscosity, suggesting that the extended conformations of PAA chains in solution are likely preserved in the thin films. We note that it is likely upon spin casting that the Na^+ ions condense close to the negatively charged carboxylate pendant groups of PAA to maintain charge neutrality, reducing the degree of chain extension in the thin films. However, a previous atomic force microscopy (AFM) study on spin-cast samples of a brush polymer with grafted PAA side chains demonstrated systematic extension in chain morphology as pH increased (*22*), corroborating our assertion that at least some level of chain extension is preserved in the solid-state films. In contrast, the viscosities of PVP solutions and the film thicknesses for spin-cast PVP samples remained unchanged across the pH range, as expected (fig. S5B).

Because of the inherent difficulty of performing nanoindentation (*23*, *24*) on nanoscale spin-cast films, micrometer-thick blade-coated PAA (MW, 450,000; atactic) films (*25*) were used for elastic modulus (*E*) measurement (fig. S6). As shown in Fig. 2B, elastic modulus increased from 10.96 ± 0.07 GPa at pH 1 to 28.53 ± 0.83 GPa at pH 12. A similar chain stiffening effect caused by reduced chain segmental mobility due to strong ionic interactions between the negatively charged polymer chains and the surrounding positive cationic coordination sphere (*26*) is generally attributed for the large increase in glass transition temperature (T_g) of

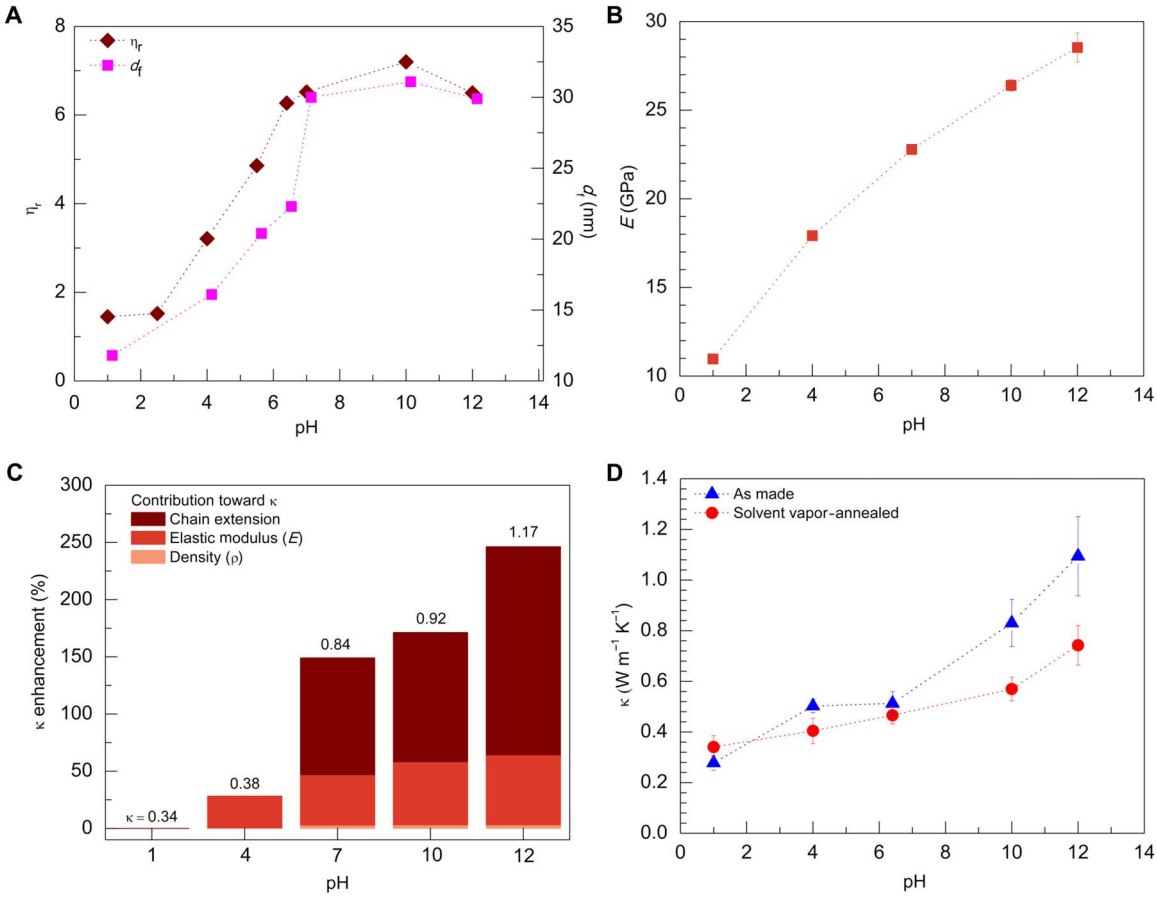

Fig. 2. Effects of PAA ionization and their contributions toward enhancement in κ. (**A**) Relative viscosity, η_r ($=\eta_{polymer}/\eta_{water}$; $\eta_{water} = 10^{-3}$ Pa·s), of a 2 wt % solution of PAA and film thickness, d_f, of spin-cast samples (from 0.5 wt % solution) as a function of pH. (**B**) Elastic modulus of blade-coated PAA (MW, 450,000) films measured by nanoindentation. The error bar shows SD of measurements at four different points on the film. (**C**) Contributions from the three ionization-induced effects toward enhancement in thermal conductivity of spin-cast PAA films. κ at different pH is noted above the bars. (**D**) Thermal conductivities of solvent vapor–annealed PAA films compared to those of as-made samples. PAA films were solvent vapor–annealed at 90°C for 30 min, followed by thermal annealing at 100°C for 15 min.

PAA with ionization (*27*). Film porosity data, measured by positronium annihilation lifetime spectroscopy (PALS) (fig. S7), showed a 33% drop from pH 4 to 12, which is consistent with the trend of ionization-dependent bulk density for partially ionized PAA (*28*).

Furthermore, grazing incidence x-ray diffraction (GI-XRD) measurements carried out on spin-cast PAA films did not show any sign of polymer crystallinity (fig. S8), thereby ruling out any crystallinity-related contribution to the measured thermal conductivity. A broad diffused peak, known as amorphous halo, can be seen for all samples, which is characteristic of amorphous polymers including PAA (*29*) and PAA salts (*30*).

Film morphology and contributions from NaOH inclusions

To rule out the possible contributions of NaOH crystals that could potentially act as high-κ fillers to measured thermal conductivity, we calculated the maximum possible volume fraction of NaOH crystals (V_{NaOH}) in the resulting polymer films (see the Supplementary Materials). These NaOH crystals formed from residual Na^+ and OH^- ions in the polymer solution could act as high-κ fillers and contribute to thermal conductivity enhancement. However, on the basis of the known amount of PAA and NaOH added in the polymer solutions at various pH, the calculated V_{NaOH} was found to be negligible (V_{NaOH} ~1.65% for the highest pH 12 sample) except for an additional sample (not shown in the data of Figs. 1B and 2), for which excess NaOH was added specifically to probe the potential contribution of NaOH crystals (shown in Fig. 3, A and B). Although crystals were not observed in the samples except for the one with excess NaOH, a Maxwell model was nevertheless used to predict the thermal conductivities that would be expected if the NaOH crystals were homogeneously distributed within the film as nanosized spherical fillers (*31*), for comparison with values measured for chain-extended PAA films. A volumetric percolation threshold equal to 25% is required for appreciable κ enhancement in these composites; this is not reached even for the highest pH PAA film (pH 12; V_{NaOH} = 1.65%). The fact that the measured PAA thermal conductivities are significantly greater than Maxwell-predicted values (Fig. 3C) indicates that κ enhancement due to ionization-induced effects dominates over the possible contributions of high-κ fillers over the range of pH selected.

Tapping-mode AFM and scanning electron microscopy (SEM) analyses of the PAA films further corroborate the theoretical calculation of V_{NaOH}. As can be seen in Fig. 3A (also see fig. S9A), AFM topography images show a smooth featureless film surface morphology for pH values up to 12. Small spherical NaOH crystals can be seen in the thin film spin-cast from polymer solution with excess NaOH added. SEM images were used to confirm surface morphology and to investigate the potential presence of NaOH crystals buried within the film (Fig. 3B and fig. S9B). We did not observe any sign of NaOH crystals except for the sample with excess NaOH added, which is consistent with the AFM topography images. Focused ion beam (FIB)–assisted cross-sectional SEM for a pH 10 sample did not show any NaOH crystal beneath the gold heater lines, ruling out the possibility of preferential crystallization of NaOH due to heterogeneous nucleation (*32*) at the metal-polymer interface (fig. S10).

Factors contributing to enhanced κ

To deconvolute the contributions to measured κ from the three ionization-induced effects, we used the minimum thermal conductivity model (MTCM) (*10*, *33*), which describes thermal transport in amorphous and highly disordered materials. According to this model, κ scales with atomic density (ρ_{atom}) as $\rho_{atom}^{1/6}$, which has been approximated with mass density (ρ) here, and linearly with sound velocity, which further depends on elastic modulus as $E^{1/2}$. Because the film density cannot be directly calculated from the PALS data, we interpolated densities at different degrees of ionization based on the bulk densities reported (*28*). By assuming that film density scales linearly with bulk density, a ~20% higher bulk density at pH 12 (α = 92.5%) compared to pH 1 (α = 0%) suggests a relatively small (~3%) density-related contribution to the enhanced κ. The modulus-related contribution to the measured κ was calculated to be ~61%. On the basis of only the density- and modulus-related contributions to κ, the thermal conductivity at pH 12 is predicted to be ~0.56 W m^{-1} K^{-1}, a ~65% enhancement in κ over that of pH 1 sample (κ = 0.34 W m^{-1} K^{-1}) that is substantially smaller than the ~250% enhancement measured. Conversely, if enhancement in κ for the spin-cast thin films were to be attributed solely to an enhancement in modulus, the elastic modulus of the pH 12 film amounts to be ~130 GPa, which is unphysical for PAA. Figure 2C shows the various contributions to measured κ for each pH calculated by taking κ for pH 1 as the baseline. We note that the measured value (κ = 0.38 ± 0.04 W m^{-1} K^{-1}) for a pH 4 sample is lower than the MTCM-calculated value (0.43 W m^{-1} K^{-1}), which is consistent with the minuscule ionization and, therefore, chain extension in spin-cast film at this pH. The MTCM, which is based on vibrational states that are neither fully localized nor propagating (diffusons), does not entirely capture the enhancement in κ measured in this system. We speculate that the extended and stiffened PAA chains may result in increased diffusion lengths for diffusons. Because long-range propagating modes have been previously shown to exist in disordered solids like amorphous Si (*13*, *34*), it is also possible that a small population of "propagons" exists in the chain-extended PAA. However, further studies are necessary to understand the detailed heat transport mechanisms in these extended systems. We note that a previous work (*35*) has examined the thermal conductivity of ionically cross-linked polymer salts, with κ reaching 0.67 W m^{-1} K^{-1}; thus, we attribute the additional κ enhancements shown in this study to the added chain extension effect in spin-cast NaOH-treated PAA thin films, which gives rise to a greater persistence length and larger effective rigidity of the polymer chains (*20*). It is likely that the predominant vibrational transfer of heat along the covalently bonded polymer backbone afforded by the extended and stiffened chain morphology as well as enhanced interchain conductance due to stronger ionic bonds result in the substantial increment in κ. The measured increases in κ are consistent with a recent computational study that predicts large enhancements in κ with increasing persistence length in amorphous polyethylene (*36*). To further confirm the contributions of extended chain morphology of the ionized PAA chains to measured thermal conductivity, we performed solvent vapor annealing (SVA) on spin-cast PAA films. Absorption of solvent vapors during SVA increases chain mobility, resulting in morphological equilibration of the polymer chains that had been kinetically frozen (*37*, *38*). As shown in Fig. 2D, the differences in thermal conductivity between "as-made" and "solvent vapor–annealed" samples are within experimental uncertainties for low pH samples, indicating that any disruption of ionic and H-bond interactions due to solvent annealing does not significantly change κ. However, for pH 10 and 12 samples, much lower thermal conductivities were measured for solvent-annealed samples, which can be explained by the coiling up (that is, relaxation) of PAA chains during the solvent annealing process. Specifically at pH 12, thermal conductivity dropped by as much as ~32%. This signifies that kinetically frozen

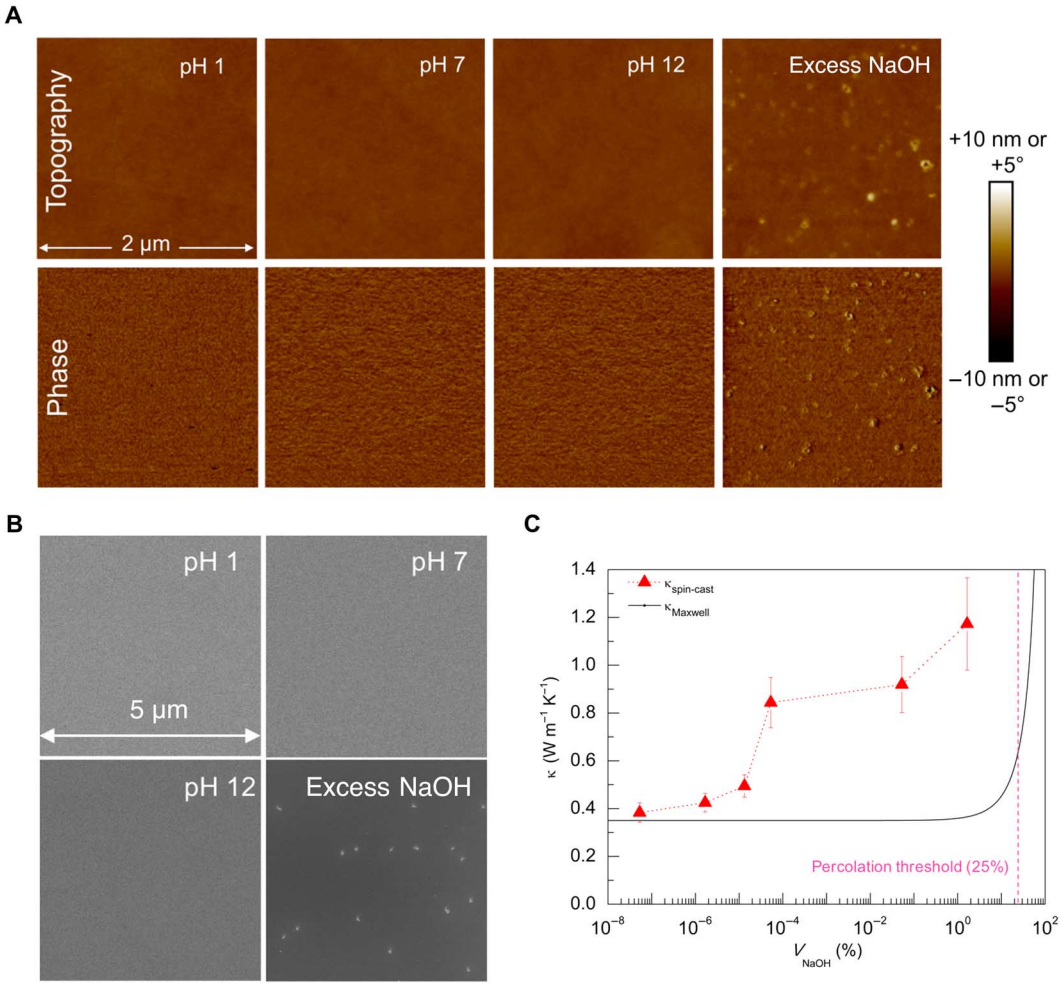

Fig. 3. Tapping-mode AFM and SEM analyses of PAA films. (**A**) Tapping-mode topography (top) and phase (bottom) images (2 μm × 2 μm) of PAA films spin-cast from solutions of different pH. AFM images have been shifted to zero mean values (that is, "flattened") for illustration purposes. Nanosized NaOH crystals are only visible in sample with excess amount of NaOH added to the PAA solution. (**B**) SEM images of the same films analyzed by AFM. NaOH crystals can be seen only when excess NaOH is added, consistent with the AFM data. (**C**) Measured thermal conductivities, $\kappa_{spin\text{-}cast}$, for spin-cast films greatly exceed the Maxwell model–predicted values, indicating that enhancement is not primarily due to a high-κ filler effect.

extended PAA chains are partially responsible for high thermal conductivities measured in the spin-cast films.

Comparison with composites

We compared the thermal conductivities of chain-extended PAA films with those of the two types of composite films, PAA/NaCl and PVP/NaOH, composed of mutually unreactive polymer-salt mixtures. We assume that the salt added in these samples is proportionally retained in the thin film upon spin casting from the polymer-salt solution and acts as a high-κ filler. As shown in Fig. 4A, salt fillers have minuscule effect on composite thermal conductivities until ~20% filler volume fraction. This signifies that extended chain morphology may be more effective at transferring heat than composite strategies, where large thermal resistances may exist at filler-filler and filler-polymer interfaces.

Micrometer-thick amorphous films

We fabricated ~1.5- to 5.5-μm-thick PAA (MW, 450,000; atactic) films by blade coating (*25*), which is a method representative of the large-scale roll-to-roll processing. The average κ measured for high pH samples (pH 7 to 12) was ~0.59 W m^{-1} K^{-1}, which is nearly 80% enhancement over the average κ (~0.33 W m^{-1} K^{-1}) measured for the pH 1 samples (Fig. 4B). The lower κ in the blade-coated samples likely results from the thermodynamic nature of the blade coating method. We note that the thermal conductivities of blade-coated high pH samples match closely with those measured for ionically cross-linked PAA films (*34*), indicating a thermal conductivity enhancement that can be largely ascribed to elastic modulus– and density-related contributions. This is in line with the slow evaporation process during blade coating that allows the chains to relax into a more thermodynamically favorable coiled-up morphology, as opposed to spin casting that freezes the polymer chains in an extended high energy state upon rapid solvent evaporation. This is further consistent with the decline in κ observed for the spin-cast films subjected to SVA that relaxes the extended chain morphology. The highest κ (0.62 ± 0.02 W m^{-1} K^{-1}) measured among the thick films is more than 50% larger than the κ (~0.4 W m^{-1} K^{-1}) achieved in unstretched ultrahigh MW semicrystalline (crystallinity, ~15%) polyethylene films of comparable thickness (*39*). The maximum value of V_{NaOH} in these films was calculated to be only 1.64%

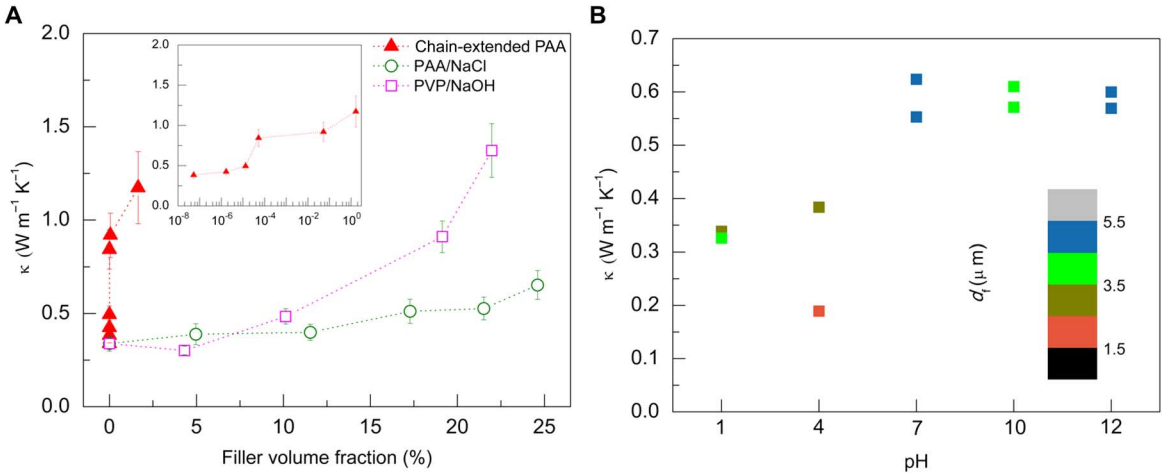

Fig. 4. Comparison of thermal conductivities of chain-extended PAA and polymer-salt composites. (**A**) Thermal conductivity of thin films of water-soluble polymers with added inorganic salts. Chain-extended PAA refers to PAA films spin-cast from solutions at different pH. Salts added in PAA/NaCl and PVP/NaOH samples do not react with respective polymers and act as high-κ fillers. The inset shows data for chain-extended PAA, with abscissa on log scale. (**B**) Thermal conductivity of thick PAA films blade-coated from solutions at different pH. The color map shows film thicknesses in micrometers. The error in κ was less than 4% for all samples and is not shown.

(corresponding to pH 12). The measured thermal conductivities for these films at high pH (that is, pH >7) significantly exceed the Maxwell-predicted values (fig. S11), ruling out any contribution to κ from NaOH crystals. Although directional shear force during blade coating can potentially lead to some short-range ordering parallel to the substrate within the polymer films, as has been previously reported for atactic PAA (*40*, *41*), any such ordering in the in-plane direction would likely cause the in-plane κ (κ_x) to be even greater than the measured cross-plane κ (κ_z). We also note that no such short-range ordering is deemed possible in the spin-cast films because of the kinetic nature of film formation.

DISCUSSION

In summary, we have used electrostatic repulsive forces to stretch the polyelectrolyte backbone at the molecular level, resulting in extended conformations, better packed chains, and enhanced modulus, all of which contribute to significantly enhanced thermal conductivities. For the spin-cast thin films, it is to be noted that centrifugal forces during spin casting may cause polymer chains to be more expanded in the in-plane direction, possibly making in-plane thermal conductivity even greater than the measured cross-plane κ (*6*). This unexplored route for molecular engineering of polymer thermal conductivity is also extended to making micrometer-thick blade-coated films, with thermal conductivity reaching more than 0.6 W m^{-1} K^{-1}.

MATERIALS AND METHODS

Experimental design

The objectives of this study were to recognize the structural bottlenecks to high thermal conductivities in amorphous polymers and to design and develop a polymeric material to address them. Two water-soluble polymers with and without ionizable pendant groups were chosen to compare and contrast the effects of polymer ionization on their thermal transport properties. Material evaluation involved thermal conductivity measurement on spin-cast thin films and materials characterization in terms of degree of polymer ionization, viscosity, film density, and elastic modulus. The materials properties were correlated with the measured thermal conductivity of the polymers. Morphological and theoretical analyses were done to rule out any extraneous contribution to measured high thermal conductivities. Additional salt composite films and thick films were fabricated to highlight the efficacy of the reported molecular design strategy to achieve high thermal conductivities in amorphous polymer films.

Sample preparation

The polymer [atactic PAA (MW, 100,000) or atactic PVP (MW, 40,000)] was dissolved in DI water, and the solution pH was adjusted to desired values by addition of 1 M HCl or 1 M NaOH. The final solution concentration was then made up to 0.5 wt % (PAA) or 1 wt % (PVP). The final solution pH was checked using pH strips. Polymer solutions were then spin-cast on precleaned Si wafers (~100 nm SiO_2 layer) at 1500 rpm for 30 s, and the resulting films were annealed at 100°C for 1 hour. Spin-casting and annealing steps were done in a glove box under nitrogen atmosphere. The blade-coated samples were prepared on a computer-controlled blade coater (model MS-1-24, Newmark Systems Inc.). Briefly, the required amount of polymer solution was placed on the substrate, which was kept on a hot plate at 90°C. Blade height was then adjusted to give the desired thickness and coating speed was set to 0.02 mm s^{-1}. The coated films were annealed at 100°C for 1 to 2 hours. Polymer-salt films were similarly prepared by first dissolving the polymers in DI water and then adding salt solution to attain the desired salt content. Further details about sample preparation are provided in the Supplementary Materials.

Thermal conductivity measurement

To prepare samples for 3ω measurement, a part of the spin- or blade-coated film was removed using a steel blade, and the cleared area was further cleaned by a cotton swab dipped in water and ethanol to give a clean polymer-free reference region. Thin heater lines were deposited using a shadow mask (50 μm) and electron beam deposition (5 nm Ti/200 nm Au) on both sample and reference regions. To test the potential dependence of measured thermal conductivity on ambient humidity, a second series of spin-coated samples also included a 50 nm thick alumina capping layer that was sputter-coated on the polymer

layer before the metal heater lines were deposited. Error analyses for the 3ω data are described in the Supplementary Materials. The film thicknesses of spin-cast films were measured by ellipsometry (Woollam M-2000DI Ellipsometer) and profilometry (Dektak XT Surface Profilometer). Only the latter was used for the blade-coated films because of their increased surface roughness.

Polymer characterizations

FTIR spectra were obtained on a Nicolet 6700 spectrometer with a grazing incidence of 85°. Polymer solution viscosity was measured on TA Instruments Advantage Rheology G2 with a steel cone of 40 mm in diameter and cone angle of 2°. Different shear rates were used to get reliable viscosity data. Film porosity was measured by PALS using a focused positron beam with implantation energy of 0.7 keV. GI-XRD measurements were carried out on a Rigaku Ultima IV x-ray diffractometer at an incident angle of 0.2°. Elastic modulus for the blade-coated films was measured on Hysitron 950 TriboIndenter equipped with a Berkovich probe and at a fixed displacement of 400 nm. Tapping-mode AFM (Bruker ICON AFM) and SEM FEI Nova 200 Nanolab SEM were used to study film morphologies. FIB-assisted SEM (FEI Nova 200 Nanolab SEM) was used to image the cross sections of PAA films beneath the gold heater lines. Further details about the measurement techniques and data analyses are provided in the Supplementary Materials.

SUPPLEMENTARY MATERIALS

Supplementary material for this article is available at http://advances.sciencemag.org/cgi/content/full/3/7/e1700342/DC1

Supplementary Text

fig. S1. Differential 3ω measurement of thermal conductivity (κ).

fig. S2. Widths measured for 40 heater lines and film thicknesses measured for 20 spin-cast PAA samples.

fig. S3. Thermal boundary conductance analysis and minimum κ.

fig. S4. Representative FTIR spectra for PAA with deconvoluted peaks.

fig. S5. Characterization of PVP films and solutions.

fig. S6. A typical force versus displacement curve from nanoindentation of a blade-coated PAA (pH 4) film.

fig. S7. PALS data for PAA films at different pH.

fig. S8. GI-XRD spectra of PAA films at different pH.

fig. S9. Tapping-mode AFM topography and phase images, as well as SEM images of spin-cast PAA films.

fig. S10. Cross-sectional view of a pH 10 PAA film under the Au heater lines.

fig. S11. Comparison of thermal conductivities of blade-coated films with Maxwell model.

fig. S12. Film thicknesses for PAA spin-cast films before (that is, in the due course of sample preparation and measurement) and right after annealing at 100°C for 45 min.

References (*42*–*55*)

REFERENCES AND NOTES

1. H. Chen, V. V. Ginzberg, J. Yang, Y. Yang, W. Liu, Y. Huang, L. Du, B. Chen, Thermal conductivity of polymer-based composites: Fundamentals and applications. *Prog. Polym. Sci.* **59**, 41–85 (2016).
2. S. Gelin, H. Tanaka, A. Lemaitre, Anomalous phonon scattering and elastic correlations in amorphous solids. *Nat. Mater.* **15**, 1177–1181 (2016).
3. A. Henry, G. Chen, High thermal conductivity of single polyethylene chains using molecular dynamics simulations. *Phys. Rev. Lett.* **101**, 235502 (2008).
4. S. Shen, A. Henry, J. Tong, R. T. Zheng, G. Chen, Polyethylene nanofibers with very high thermal conductivities. *Nat. Nanotechnol.* **5**, 251–255 (2010).
5. C. L. Choy, Thermal conductivity of polymers. *Polymer* **18**, 984–1004 (1977).
6. K. Kurabayashi, M. Asheghi, M. Touzelbaev, K. E. Goodson, Measurement of the thermal conductivity anisotropy in polyimide films. *J. Microelectromech. Syst.* **8**, 180–191 (1999).
7. V. Singh, T. L. Bougher, A. Weathers, Y. Cai, K. Bi, M. T. Pettes, S. A. McMenamin, W. Lv, D. P. Resler, T. R. Gattuso, D. H. Altman, K. H. Sandhage, L. Shi, A. Henry, B. A. Cola, High thermal conductivity of chain-oriented amorphous polythiophene. *Nat. Nanotechnol.* **9**, 384–390 (2014).
8. A. Roy, T. L. Bougher, R. Geng, Y. Ke, J. Locklin, B. A. Cola, Thermal conductance of poly(3-methylthiophene) brushes. *ACS Appl. Mater. Interfaces* **8**, 25578–25585 (2016).
9. M. D. Losego, L. Moh, K. A. Arpin, D. G. Cahill, P. V. Braun, Interfacial thermal conductance in spun-cast polymer films and polymer brushes. *Appl. Phys. Lett.* **97**, 011908 (2010).
10. W.-P. Hsieh, M. D. Losego, P. V. Braun, S. Shenogin, P. Keblinski, D. G. Cahill, Testing the minimum thermal conductivity model for amorphous polymers using high pressure. *Phys. Rev. B* **83**, 174205 (2011).
11. P. B. Allen, J. L. Feldman, J. Fabian, F. Wooten, Diffusons, locons and propagons: Character of atomic vibrations in amorphous Si. *Philos. Mag. B* **79**, 1715–1731 (1999).
12. S. Shenogin, A. Bodapati, P. Keblinski, A. J. H. McGaughey, Predicting the thermal conductivity of inorganic and polymeric glasses: The role of anharmonicity. *J. Appl. Phys.* **105**, 034906 (2009).
13. K. T. Regner, D. P. Sellan, S. Zonghui, C. H. Amon, A. J. H. McGaughey, A. J. Malen, Broadband phonon mean free path contributions to thermal conductivity measured using frequency domain thermoreflectance. *Nat. Commun.* **4**, 1640 (2013).
14. A. Henry, Thermal transport in polymers. *Annu. Rev. Heat Transfer* **17**, 485–520 (2013).
15. S.-M. Lee, D. G. Cahill, Heat transport in thin dielectric films. *J. Appl. Phys.* **81**, 2590–2595 (1997).
16. T. Borca-Tasciuc, A. R. Kumar, G. Chen, Data reduction in 3ω method for thin-film thermal conductivity determination. *Rev. Sci. Instrum.* **72**, 2139–2147 (2001).
17. J. Choi, M. F. Rubner, Influence of degree of ionization on weak polyelectrolyte multilayer assembly. *Macromolecules* **38**, 116–124 (2005).
18. A. F. Xie, S. Granick, Local electrostatics within a polyelectrolyte multilayer with embedded weak polyelectrolyte. *Macromolecules* **35**, 1805–1813 (2002).
19. D. W. van Krevelen, K. Te Nijenhuis, *Properties of Polymers: Their Correlation with Chemical Structure; Their Numerical Estimation and Prediction from Additive Group Contributions* (Elsevier, ed. 4, 2009).
20. S. W. Cranford, M. J. Buehler, Variation of weak polyelectrolyte persistence length through an electrostatic contour length. *Macromolecules* **45**, 8067–8082 (2012).
21. D. Stigter, K. A. Dill, Theory of radii and second virial coefficients. 2. Weakly charged polyelectrolytes. *Macromolecules* **28**, 5338–5346 (1995).
22. H.-i. Lee, J. R. Boyce, A. Nese, S. S. Sheiko, K. Matyjaszewski, pH-induced conformational changes of loosely grafted molecular brushes containing poly(acrylic acid) side chains. *Polymer* **49**, 5490–5496 (2008).
23. W. C. Oliver, G. M. Pharr, An improved technique for determining hardness and elastic modulus. *J. Mater. Res.* **7**, 1564–1583 (1992).
24. R. Akhtar, N. Schwarzer, M. J. Sherratt, R. E. B. Watson, H. K. Graham, A. W. Trafford, P. M. Mummery, B. Derby, Nanoindentation of histological specimens: Mapping the elastic properties of soft tissues. *J. Mater. Res.* **24**, 638–646 (2009).
25. B.-G. Kim, E. J. Jeong, J. W. Chung, S. Seo, B. Koo, J. Kim, A molecular design principle of lyotropic liquid-crystalline conjugated polymers with directed alignment capability for plastic electronics. *Nat. Mater.* **12**, 659–664 (2013).
26. A. Eisenberg, Glass transitions in ionic polymers. *Macromolecules* **4**, 125–128 (1971).
27. A. Eisenberg, H. Matsura, T. Yokoyama, Glass transition in ionic polymers: The acrylates. *J. Polym. Sci. B* **9**, 2131–2135 (1971).
28. K. Hiraoka, H. Shin, T. Yokoyama, Density measurements of poly(acrylic acid) sodium salts. *Polym. Bull.* **8**, 303–309 (1982).
29. M. Todica, T. Stefan, S. Simon, I. Balasz, L. Daraban, UV-vis and XRD investigation of graphite-doped poly(acrylic) acid membranes. *Turk. J. Phys.* **38**, 261–267 (2014).
30. S. Komaba, N. Yabuuchi, T. Ozeki, Z.-J. Han, K. Shimomura, H. Yui, Y. Katayama, T. Miura, Comparative study of sodium polyacrylate and poly(vinylidene fluoride) as binders for high capacity Si-graphite composite negative electrodes in Li-ion batteries. *J. Phys. Chem. C* **116**, 1380–1389 (2012).
31. V. R. Raghavan, H. Martin, Modelling of two-phase thermal conductivity. *Chem. Eng. Process.* **34**, 439–446 (1995).
32. T. Brar, P. France, P. G. Smirniotis, Heterogeneous versus homogeneous nucleation and growth of zeolite A. *J. Phys. Chem. B* **105**, 5383–5390 (2001).
33. X. Xie, D. Li, T.-H. Tsai, J. Liu, P. V. Braun, D. G. Cahill, Thermal conductivity, heat capacity, and elastic constants of water soluble polymers and polymer blends. *Macromolecules* **49**, 972–978 (2016).
34. X. Liu, J. L. Feldman, D. G. Cahill, R. S. Crandall, N. Bernstein, D. M. Photiadis, M. J. Mehl, D. A. Papaconstantopoulos, High thermal conductivity of a hydrogenated amorphous silicon film. *Phys. Rev. Lett.* **102**, 035901 (2009).
35. X. Xie, K. Yang, D. Li, T.-H. Tsai, J. Shin, P. V. Braun, D. G. Cahill, High and low thermal conductivity of amorphous macromolecules. *Phys. Rev. B* **95**, 035406 (2017).
36. T. Zhang, T. Luo, Role of chain morphology and stiffness in thermal conductivity of amorphous polymers. *J. Phys. Chem. B* **120**, 803–812 (2016).
37. J. Vogelsang, J. Brazard, T. Adachi, J. C. Bolinger, P. F. Barbara, Watching the annealing process one polymer chain at a time. *Angew. Chem.* **123**, 2305–2309 (2011).
38. Y. S. Jung, C. A. Ross, Solvent-vapor-induced tunability of self-assembled block copolymer patterns. *Adv. Mater.* **21**, 2540–2545 (2009).

39. H. Ghasemi, T. Nagarajan, X. Huang, J. Loomis, X. Li, J. Tong, J. Wang, G. Chen, High thermal conductivity ultra-high molecular weight polyethylene (UHMWPE) films, in *Fourteenth Intersociety Conference on Thermal and Thermomechanical Phenomena in Electronic Systems (ITherm)* (IEEE, 2014), pp. 235–239.
40. V. A. Kargin, S. Y. Mirlina, V. A. Kabanov, G. A. Mikheleva, A study of the structure of isotactic polyacrylic acid and its salts. *Vysokomol. Soedin.* **3**, 139–143 (1961).
41. M. L. Miller, K. O'Donnell, J. Skogman, Crystalline polyacrylic acid. *J. Colloid Sci.* **17**, 649–659 (1962).
42. D. G. Cahill, Thermal-conductivity measurement from 30K to 750K: The 3ω method. *Rev. Sci. Instrum.* **61**, 802–808 (1990).
43. T. Borca-Tasciuc, D. Song, J. L. Liu, G. Chen, K. L. Wang, X. Sun, M. S. Dresselhaus, T. Radetic, R. Gronsky, Anisotropic thermal conductivity of a Si/Ge superlattice. *Mater. Res. Soc. Symp. Proc.* **545**, 473 (1998).
44. Y. K. Koh, S. L. Singer, W. Kim, J. M. O. Zide, H. Lu, D. G. Cahill, A. Majumdar, A. C. Gossard, Comparison of the 3ω method and time-domain thermoreflectance for measurements of the cross-plane thermal conductivity of epitaxial semiconductors. *J. Appl. Phys.* **105**, 054303 (2009).
45. A. Richter, R. Guico, J. Wang, Calibrating an ellipsometer using x-ray reflectivity. *Rev. Sci. Instrum.* **72**, 3004–3007 (2001).
46. B. Armstrong, *Dektak XT: Standard Operating Procedure* (2014).
47. J. Liu, S. Ju, Y. Ding, R. Yang, Size effect on the thermal conductivity of ultrathin polystyrene films size effect on the thermal conductivity of ultrathin polystyrene films. *Appl. Phys. Lett.* **104**, 153110 (2014).
48. K. Zheng, F. Sun, X. Tian, J. Zhu, Y. Ma, D. Tang, F. Wang, Tuning the interfacial thermal conductance between polystyrene and sapphire by controlling the interfacial adhesion. *ACS Appl. Mater. Interfaces* **7**, 23644–23649 (2015).
49. R. J. Stevens, A. N. Smith, P. M. Norris, Measurement of thermal boundary conductance of a series of metal-dielectric interfaces by the transient thermoreflectance technique. *J. Heat Transfer* **127**, 315–322 (2016).
50. K. Zheng, F. Sun, J. Zhu, Y. Ma, X. Li, D. Tang, F. Wang, X. Wang, Enhancing the thermal conductance of polymer and sapphire interface via self-assembled monolayer. *ACS Nano* **10**, 7792–7798 (2016).
51. K. Zheng, J. Zhu, Y.-M. Ma, D.-W. Tang, F.-S. Wang, Interfacial thermal resistance between high-density polyethylene (HDPE) and sapphire. *Chin. Phys. B* **23**, 107307 (2014).
52. A. B. Unni, G. Vignaud, J. P. Chapel, J. Giermanska, J. K. Bal, N. Delorme, T. Beuvier, S. Thomas, Y. Grohens, A. Gibaud, Probing the density variation of confined polymer thin films via simple model-independent nanoparticle adsorption. *Macromolecules* **50**, 1027–1036 (2017).
53. D. W. Gidley, H.-G. Peng, R. S. Vallery, Positron annihilation as a method to characterize porous materials. *Annu. Rev. Mater. Res.* **36**, 49–79 (2006).
54. S. N. Magonov, V. Elings, M. H. Whangbo, Phase imaging and stiffness in tapping-mode atomic force microscopy. *Surf. Sci.* **375**, 385–391 (1997).
55. J. Pawley, Low voltage scanning electron microscopy. *J. Microsc.* **136**, 45–68 (1984).

Acknowledgments: We acknowledge the Lurie Nanofabrication Facility and the Michigan Center for Materials Characterization for sample preparation and characterization. A.S. acknowledges Z. Li and H. Sun for help with the GI-XRD and nanoindentation measurements, respectively. C.L. acknowledges A. Hunter for help with the SEM and FIB-SEM analyses. **Funding:** A.S. acknowledges support from the Rackham Predoctoral Fellowship Program from the University of Michigan, Ann Arbor. G.-H.K. acknowledges a postdoctoral fellowship from the University of Michigan Energy Institute. **Author contributions:** A.S. conceived the initial ideas and designed the experiments with the help of J.K. A.S. prepared the polymer thin-film samples with the help of C.L. and G.-H.K. A.S. and G.-H.K. confirmed the initial hypothesis. A.S. prepared samples for and measured and analyzed FTIR, viscosity, nanoindentation, and GI-XRD data. C.L. measured and analyzed thermal conductivity, with initial help from G.-H.K., and performed SEM, AFM, and FIB-SEM characterizations. A.S. and C.L. prepared blade-coated films for thermal conductivity measurements. D.G. measured PALS. K.P.P. and J.K. supervised the work. A.S. wrote the manuscript, with contributions from C.L. K.P.P. and J.K. revised the manuscript. All authors provided feedback on the manuscript. **Competing interests:** J.K., C.L., A.S., K.P.P., and G.-H.K. are authors on a provisional patent application related to this work (U.S. Provisional Application #62/517,487; filed on 9 June 2017). D.G. declares that he has no competing interests. **Data and materials availability:** All data needed to evaluate the conclusions in the paper are present in the paper and/or the Supplementary Materials. Additional data related to this paper may be requested from the authors.

Submitted 1 February 2017
Accepted 26 June 2017
Published 28 July 2017
10.1126/sciadv.1700342

Citation: A. Shanker, C. Li, G.-H. Kim, D. Gidley, K. P. Pipe, J. Kim, High thermal conductivity in electrostatically engineered amorphous polymers. *Sci. Adv.* **3**, e1700342 (2017).

ScienceAdvances

High thermal conductivity in electrostatically engineered amorphous polymers

Apoorv Shanker, Chen Li, Gun-Ho Kim, David Gidley, Kevin P. Pipe and Jinsang Kim

Sci Adv **3** (7), e1700342.
DOI: 10.1126/sciadv.1700342